Journal of Cardiovascular Translational Research (2022) 15:167–178
https://doi.org/10.1007/s12265-021-10153-5

ORIGINAL ARTICLE

Intracellular Ca^{2+} Dysregulation in Coronary Smooth Muscle Is Similar in Coronary Disease of Humans and Ossabaw Miniature Swine

Jill K. Badin[1] · Caleb Eggenberger[1,2] · Stacey Dineen Rodenbeck[1,3] · Zubair A. Hashmi[4] · I-wen Wang[4] · Jose P. Garcia[4] · Mouhamad Alloosh[1] · Michael Sturek[1]

Received: 30 December 2020 / Accepted: 2 July 2021 / Published online: 20 July 2021

Abstract

Intracellular free Ca^{2+} ($[Ca^{2+}]_i$) dysregulation occurs in coronary smooth muscle (CSM) in atherosclerotic coronary artery disease (CAD) of metabolic syndrome (MetS) swine. Our goal was to determine how CAD severity, arterial structure, and MetS risk factors associate with $[Ca^{2+}]_i$ dysregulation in human CAD compared to changes in Ossabaw miniature swine. CSM cells were dispersed from coronary arteries of explanted hearts from transplant recipients and from lean and MetS swine with CAD. CSM $[Ca^{2+}]_i$ elicited by Ca^{2+} influx and sarcoplasmic reticulum (SR) Ca^{2+} release and sequestration was measured with fura-2. Increased $[Ca^{2+}]_i$ signaling was associated with advanced age and a greater media area in human CAD. Decreased $[Ca^{2+}]_i$ signaling was associated with a greater number of risk factors and a higher plaque burden in human and swine CAD. Similar $[Ca^{2+}]_i$ dysregulation exhibited in human and Ossabaw swine CSM provides strong evidence for the translational relevance of this large animal model.

Keywords Atherosclerosis · Obesity · Metabolic syndrome · Histology · Sarco-endoplasmic reticulum Ca^{2+} ATPase · Ca^{2+} influx · Ca^{2+} release · Animal model · Risk factors

Introduction

Metabolic syndrome (MetS) is characterized by a clustering of three or more of the following five conditions: central obesity, hypertension, dyslipidemia, insulin resistance, and glucose intolerance [1]. MetS affects one-third of all adults in the USA and increases the risk of developing coronary artery disease (CAD), which continues to be the primary cause of mortality worldwide and accounts for 1 in 7 deaths in the USA [1]. CAD-induced ischemic cardiomyopathy is the leading cause of heart failure, followed by dilated non-ischemic cardiomyopathy, hypertension, and valvular heart disease [2].

CAD is a progressive disease where initial endothelial damage leads to lipid and inflammatory cell infiltration of the arterial wall, causing medial thickening and neointima formation [3]. This arterial restructuring is exacerbated by the proliferation and recruitment of coronary smooth muscle (CSM) cells to the plaque, which is accomplished by the phenotypic switching of CSM from a differentiated, contractile phenotype to a proliferative, migratory phenotype [4]. These migratory CSM cells secrete and deposit extracellular matrix like collagen, elastin, and fibrin into the thickening artery wall. While the presence of CSM inside the plaque contributes to

Associate Editor Adrian Chester oversaw the review of this article

✉ Michael Sturek
msturek@iu.edu

[1] Department of Anatomy, Cell Biology, & Physiology, Indiana University School of Medicine, 635 Barnhill Dr., Medical Sciences, Room 385, Indianapolis, IN 46202, USA

[2] Marian University College of Osteopathic Medicine, Indianapolis, IN 46222, USA

[3] Department of Biology, Harding University, Searcy, AR 72149, USA

[4] Cardiothoracic Transplantation Surgery, Indiana University - Methodist Hospital, Indianapolis, IN 46202, USA

plaque stability, over time, the accumulation of lipid and cellular debris results in a necrotic core and plaque destabilization that often leads to plaque rupture and myocardial infarction. In one study, patients hospitalized for ST segment elevation myocardial infarction who had multivessel CAD had an 8-year mortality from heart failure rate of 11%, as opposed to only a 1% mortality rate for individuals similarly hospitalized without multivessel CAD [5]. Further, CSM dedifferentiation into an osteogenic phenotype is associated with vascular calcification, which is directly related to increased mortality and cardiac events [6], plaque instability, and rupture [7].

Ca^{2+} is a vital secondary messenger involved in the regulation of several key smooth muscle cell functions, such as transcription [8, 9], migration [10, 11], proliferation [4, 12–14], and contraction [4, 15]. Previous research (reviewed in [16]) has shown that CAD is accompanied by alterations in many CSM Ca^{2+} transporters, including voltage-gated Ca^{2+} channels [17, 18], transient receptor potential channels [19], sarco-endoplasmic reticulum Ca^{2+} ATPases [17, 19–21], plasma membrane Ca^{2+} ATPases [17], and Na^{+}/Ca^{2+} exchangers [17]. Our lab recently showed that intracellular Ca^{2+} ($[Ca^{2+}]_i$) handling alterations that accompany CAD occur in a biphasic manner in Ossabaw miniature swine, with enhanced Ca^{2+} signaling in early, mild disease and decreased Ca^{2+} signaling in late, severe disease [22]. Furthermore, when the plaque was separated from the arterial wall in diseased coronary arteries, CSM isolated exclusively from the plaque region exhibited decreased SR Ca^{2+} store and SR Ca^{2+} pump activity, while CSM isolated from the arterial wall exhibited increased SR Ca^{2+} store SR Ca^{2+} pump activity [22].

There is difficulty in finding an animal model for CAD, as there are many risk factors and uncontrollable variables in the human population. Our lab has characterized the Ossabaw miniature swine model of MetS and CAD [23]. Due to their "thrifty genotype," Ossabaw swine have a propensity to develop all characteristics of MetS when fed an atherogenic diet [24, 25]. While Ossabaw swine develop diffuse, human-like coronary plaques [21], CSM $[Ca^{2+}]_i$ handling patterns have never been compared to freshly isolated CSM from human patients. Therefore, the aims of the current study are (1) to determine how disease severity, arterial restructuring, and MetS risk factors are associated with $[Ca^{2+}]_i$ dysfunction in fresh, non-cultured human CSM and (2) to determine whether CSM $[Ca^{2+}]_i$ dysregulation in Ossabaw miniature swine is similar to CSM $[Ca^{2+}]_i$ dysregulation in human CAD patients. These results will aid in characterizing the association between pathological arterial remodeling and dysfunctional CSM $[Ca^{2+}]_i$ handling in human heart failure patients and will strengthen the Ossabaw miniature swine as a translational model for CAD pathology and at the $[Ca^{2+}]_i$ signaling level.

Materials and Methods

Collection of Human Tissue

Explanted human hearts were collected from 24 patients (15 male, 9 female; aged 51.0 ± 2.5 years) undergoing heart transplantation surgery at Methodist Hospital in Indianapolis, IN, between 2015 and 2018. Epicardial coronary arteries were dissected from the heart at the time of removal and stored for no longer than 24 h in a physiological salt solution, which preserves intracellular Ca^{2+} regulatory function (e.g., [22, 24, 25]). Intracellular Ca^{2+} measures were successfully conducted on cells from arteries of all 24 hearts. Patients were defined by histology of the coronary segments as non-ischemic or ischemic for plaque burden up to 75% and > 75%, respectively.

Animals

All experimental procedures involving animals were approved by the Institutional Animal Care and Use Committee at Indiana University School of Medicine with the recommendations outlined by the National Research Council and the American Veterinary Medical Association Panel on Euthanasia [26, 27]. Ossabaw miniature swine were fed either standard chow diet (5L80; Purina Test Diet, Richmond, IN) or a hypercaloric, atherogenic diet (n = 7 for both groups) [22, 24, 25]. Pigs were euthanized via cardiectomy, and coronary arteries were removed for further analysis.

Swine Metabolic Phenotyping

Blood was collected at time of euthanasia for analysis (ANTECH Diagnostics, Fishers, IN).

Histology

Segments from proximal epicardial arteries (2–4 mm in length) were placed in 10% phosphate-buffered formalin for 24–48 h and then transferred to 70% ethanol. The proximal epicardial arteries used for histology and intracellular Ca^{2+} measures were not bypassed previously. We assume that blood flow never was zero even in the ischemic arteries defined by the > 75% plaque burden. Histology of arterial cross sections was performed in the Department of Anatomy and Cell Biology at Indiana University School of Medicine. Verhoeff-Van Gieson elastin stain was used to determine media area and plaque burden, which we define as the percentage of the original lumen that is occupied by atherosclerotic plaque. Von Kossa stains calcified areas black to determine vascular calcification. Masson's trichrome stain was used to

visualize collagen (blue) and cellular composition (red). Images were captured with a Leica DM3000 microscope connected to Leica Application Suites V4.1 software (Leica Microsystems GmbH, Wetzlar, Germany) and analyzed using Adobe Photoshop® CS6.

Assessment of $[Ca^{2+}]_i$ Regulation

Whole-cell $[Ca^{2+}]_i$ levels were measured at room temperature (22–25 °C) by using the fluorescent Ca^{2+} indicator fura-2 AM (InCa++ Ca2+ Imaging System, Intracellular Imaging, Cincinnati, OH) as previously described [19, 21, 24, 25] and following the standards set in the field [28, 29]. Briefly, freshly dispersed smooth muscle cells from the proximal 45 mm of the left anterior descending artery were incubated with 3.0 μM fura-2 AM (Molecular Probes, Eugene, OR) to load the cells with fura-2. An aliquot of cells loaded with fura-2 was placed on a coverslip contained within a constant-flow superfusion chamber that was mounted on the microscope (model TMS-F, Nikon, Melville, NY), with flow maintained at a constant rate of 1–2 mL/min to change solutions. Basal Ca^{2+} levels were measured in physiologic salt solution. Calcium influx and maximal sarcoplasmic reticulum (SR) Ca^{2+} loading were accomplished by depolarization with high (80 mM) K^+ solution to activate voltage-gated Ca^{2+} channels. SR Ca^{2+} stores were released with 5 mM caffeine in Ca^{2+}-free solution to activate SR ryanodine receptors. A caffeine wash-out phase was used to determine sarcoendoplasmic reticulum Ca^{2+} ATPase (SERCA) function via the undershoot below baseline during this recovery period [30–32]. Fura-2 in CSM was excited by light from a 300-W xenon arc lamp that was passed through a computer-controlled filter changer containing 340-nm and 380-nm bandpass filters. Whole-cell fura-2 fluorescence was expressed as the 340 nm/380 nm ratio of fura-2 emission at 510 nm.

Statistics

Statistical analysis was performed using GraphPad Prism 5.0 (San Diego, CA). Unpaired Student's *t* test was performed for comparisons in swine and one-way analysis of variance with Newman-Keuls post hoc analysis for comparison of human groups. Data are presented as mean ± standard error. Correlations were determined using Pearson's product-moment coefficient of correlation. Simple regression analyses were performed to determine statistical significance of the correlations. Statistical significance was set at $p < 0.05$.

Results

Structure of Human and Swine Coronary Arteries

Representative histological stains for humans (Fig. 1a–f) and swine (Fig. 1g–l) are shown. Human arteries show great diversity in disease state and structure and have been grouped based on percent plaque burden (Fig. 1m–o). Figure 1m (blue symbols) illustrates the average plaque burden and variability in the three human groups. While calcification was similar between human groups due to high within-group variability (Fig. 1n), fibrosis as measured by percent collagen was increased in the ischemic > 75% plaque burden group compared to the non-ischemic < 50% plaque burden group (Fig. 1o). Similar to the human groups, swine with MetS-induced CAD exhibited increased plaque burden (Fig. 1m), similar vascular calcification (Fig. 1n), and greater collagen content (Fig. 1o) compared to their lean counterparts. The two bars on the *x*-axes of the graphs signify that statistics were done only between experimental groups of the same species.

Clinical Characteristics Are Similar in Humans with Different CAD Severities

Clinical characteristics of patients and swine are in Table 1. Heart function parameters were similar between the groups, including ejection fraction, left ventricular end-diastolic pressure, and coronary output, but only qualitatively recorded in patient records. The quantified systolic and diastolic blood pressures were not different (Table 1), which is consistent with qualitatively described similar heart function between the clinical groups. There were no sex-specific differences in any of the measured parameters. Overall, while these groups differ in CAD severity, they exhibit comparable metabolic and functional disease parameters, i.e., similar increased cardiometabolic risk above healthy controls. Swine on an atherogenic diet developed significantly higher weight, systolic blood pressure, fasting blood glucose, total cholesterol, and triglyceride levels compared to lean, healthy controls, indicative of MetS.

Disease Severity, Arterial Structure, and Metabolic Parameters Are Correlated to Changes in $[Ca^{2+}]_i$ Handling

Figure 2 shows a sample $[Ca^{2+}]_i$ tracing from a representative human CSM cell. Table 2 shows that greater CAD severity, as measured by the intima/media ratio and percent collagen [22], was significantly correlated to

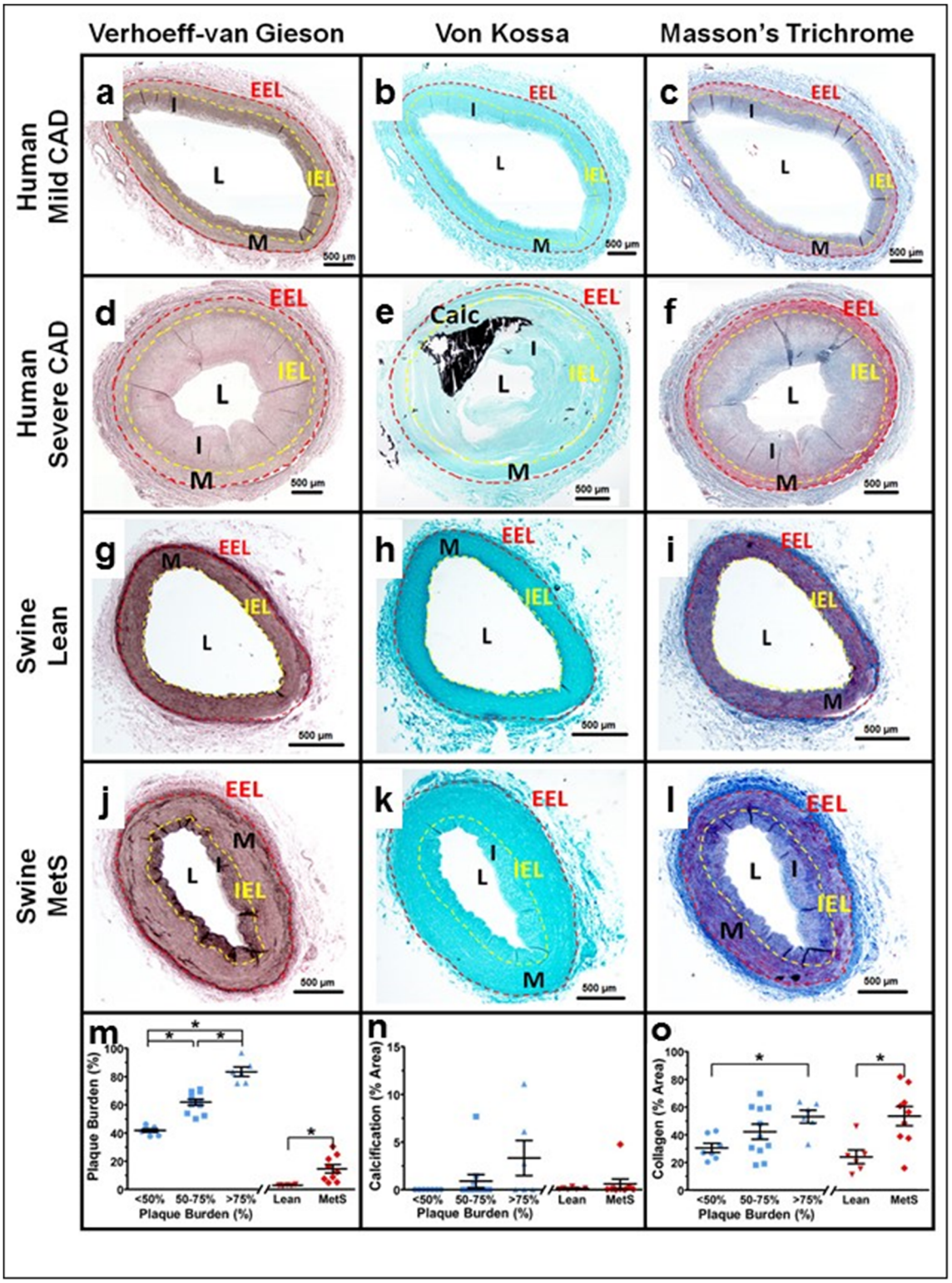
Verhoeff-van Gieson
Von Kossa
Masson's Trichrome
Human Mild CAD
Human Severe CAD
Swine Lean
Swine MetS
a
b
c
d
e
f
g
h
i
j
k
l
m
n
o
EEL
IEL
L
I
M
Calc
500 μm
Plaque Burden (%)
Calcification (% Area)
Collagen (% Area)
<50%
50-75%
>75%
Lean
MetS

◀ Fig. 1 Histological staining reveals similar pathological remodeling in both humans and swine. Coronary artery histological sections from a human with non-ischemic < 50% plaque burden (a–c), a human with an ischemic > 75% plaque burden (d–f), a lean swine (g–i), and a MetS swine (j–l). Verhoeff-Van Gieson staining was used to determine plaque burden and the areas of the tunica media and intima using the visible external elastic lamina (EEL, red dashed line) and internal elastic lamina (IEL, yellow dashed line) (a, d, g, j). Von Kossa staining was used to determine percent of vascular calcification (black) (b, e, h, k). Trichrome staining was used to determine the percent collagen (blue) (c, f, i, l). Humans (bars and blue symbols) were binned based on percent plaque burden and swine (bars and red symbols) showed significantly increased plaque burden in the MetS group compared to the lean group (m). Percent vascular calcification was not significantly different between human or swine groups (n). The percent collagen increased with disease in both the human and swine groups (o). EEL, external elastic lamina; IEL, internal elastic lamina; M, tunica media; I, tunica intima; L, lumen

decreased Ca^{2+} influx through voltage-gated Ca^{2+} channels and a decreased SR Ca^{2+} store release. In contrast to those inverse correlations, an increased media area was positively correlated to increased Ca^{2+} influx and SR Ca^{2+} store release. Increased vascular calcification was correlated to a decreased Ca^{2+} influx. Body mass index (BMI) and the number of MetS risk factors present in the patient were correlated to a decreased Ca^{2+} influx. Dyslipidemia, including increased LDL and total cholesterol levels, was correlated to decreased Ca^{2+} influx. Age was significantly correlated to an increased SR Ca^{2+} store release. Correlation graphs are presented in Figs. 3 and 4. Similar correlations on the Ossabaw miniature swine model of MetS and CAD are published [22, 24, 25].

$[Ca^{2+}]_i$ Handling in Ossabaw Swine Recapitulates $[Ca^{2+}]_i$ Handling in Human CSM in Both Health and Disease

Representative single-cell tracings of $[Ca^{2+}]i$ are shown a lean swine, MetS swine, human with mild CAD, and human with severe CAD (Fig. 5a). The $[Ca^{2+}]_i$ tracing from the human with mild CAD closely resembles the $[Ca^{2+}]_i$ from the lean swine, while the $[Ca^{2+}]_i$ tracing from the human with severe CAD closely resembles the $[Ca^{2+}]_i$ from the MetS swine. Humans with less than 50% and 50–75% plaque burden did not exhibit any differences in $[Ca^{2+}]_i$ handling, while humans with greater than 75% plaque burden had a significantly lower Ca^{2+} influx (Fig. 5b), SR Ca^{2+} store release (Fig. 5c), and undershoot (Fig. 5d). Swine with MetS-induced CAD showed remarkably similar directional changes, with a lower Ca^{2+} influx (Fig. 5b), SR Ca^{2+} store release (Fig. 5c), and undershoot (Fig. 5d) in the MetS group compared to the lean group. This clearly illustrates that similar $[Ca^{2+}]_i$ dysregulation is present in CAD in humans and Ossabaw miniature swine.

Discussion

This study provides insight into $[Ca^{2+}]_i$ handling in freshly isolated CSM from explanted hearts of human cardiomyopathy patients. We found that a thickened media layer, which is associated with mild CAD and aging in pigs [24], was correlated to enhanced $[Ca^{2+}]_i$ signaling. Advanced CAD progression, as measured by plaque burden and percent collagen, and the number of MetS/cardiometabolic risk factors, BMI, and LDL and total cholesterol levels, are correlated to decreased $[Ca^{2+}]_i$ signaling. Increased vascular calcification was accompanied by a decrease in Ca^{2+} influx. These trends exemplify that $[Ca^{2+}]_i$ regulation is compromised in patients with severe, more occlusive CAD and in patients with certain MetS risk factors. By measuring $[Ca^{2+}]_i$ from freshly dispersed, non-cultured CSM from explanted hearts of human patients, we provide novel insight into the intricacies of $[Ca^{2+}]_i$ dysregulation in diseased human CSM ex vivo and how CAD severity and certain metabolic risk factors correlate with this dysregulation. The $[Ca^{2+}]_i$ dysregulation patterns seen in Ossabaw miniature swine with MetS, CAD, and advanced age are consistent with the human data [22, 24, 25], supporting the strong clinical relevance of this large animal model on the cellular Ca^{2+} signaling level.

Recently, our lab has clarified that CSM Ca^{2+} dysregulation occurs in a biphasic manner during CAD progression, with increased $[Ca^{2+}]_i$ handling in early CAD and decreased $[Ca^{2+}]_i$ handling in late CAD [22]. Dysregulation of Ca^{2+} signaling pathways is associated with CSM dedifferentiation into a synthetic or osteogenic phenotype, which is followed by proliferation, migration to the growing neointima, and deposition of hydroxyapatite crystals in the extracellular matrix leading to vascular calcification [33]. Often, this change in phenotype occurs due to CSM adaptations to changes in the extracellular environment, such as increased reactive oxygen species and dyslipidemia [34–36].

Heart failure is a complex, heterogeneous disease with many different etiologies, risk factors, and pathophysiologies. CAD is the leading cause of heart failure and progression of CAD is related to progression of left ventricular dysfunction, a common characteristic of heart failure [37]. In the current study, we used histology obtained from the proximal segment of an epicardial coronary artery from patients with cardiomyopathy to classify their

Table 1 Clinical characteristics of human subjects and swine

	Non-ischemic		Ischemic	
Humans	**< 50% PB**	**50–75% PB**	**> 75% PB**	***p***
N	7	11	6	-
Anthropometric data				
Height (cm)	170 ± 4	176 ± 3	176 ± 4	N.S.
Weight (kg)	81 ± 6	86 ± 5	86 ± 10	N.S.
BMI (kg/m^2)	28 ± 2	27 ± 1	27 ± 2	N.S.
Clinical data				
Age (years)	52 ± 5	51 ± 4	49 ± 5	N.S.
Male/female	3/4	7/4	5/1	N.S.
SBP (mmHg)	107 ± 5	110 ± 5	104 ± 4	N.S.
DBP (mmHg)	67 ± 5	70 ± 5	69 ± 4	N.S.
Ex-smoker	2 (29%)	3 (27%)	4 (67%)	N.S.
LVAD	3 (43%)	7 (64%)	4 (67%)	N.S.
Presence of MetS	3 (43%)	4 (36%)	3 (50%)	N.S.
No. MetS risk factors	1.9 ± 0.7	2.1 ± 0.4	2.5 ± 0.6	N.S.
Biochemistry data				
Fasting bG (mg/dL)	128 ± 18	106 ± 15	106 ± 10	N.S.
HbA1c (%)	5.6 ± 0.2	5.5 ± 0.1	5.0 ± 0.3	N.S.
Total cholesterol (mg/dL)	139 ± 7	161 ± 20	136 ± 18	N.S.
LDL (mg/dL)	75 ± 7	97 ± 17	81 ± 18	N.S.
HDL (mg/dL)	40 ± 4	38 ± 4	34 ± 2	N.S.
LDL/HDL ratio	2.0 ± 0.2	2.7 ± 0.4	2.3 ± 0.5	N.S.
Triglycerides (mg/dL)	117 ± 19	128 ± 14	108 ± 13	N.S.
Comorbidities				
Atrial fibrillation	2 (29%)	5 (45%)	3 (50%)	N.S.
Diabetes mellitus	2 (29%)	2 (18%)	0 (0%)	N.S.
Kidney disease	3 (43%)	3 (27%)	1 (17%)	N.S.
Cancer	1 (14%)	1 (9%)	0 (0%)	N.S.
Clinical depression	3 (43%)	3 (27%)	4 (67%)	N.S.
Treatments				
Aspirin	4 (57%)	10 (91%)	3 (50%)	N.S.
ACEI/ARB	2 (29%)	4 (36%)	2 (33%)	N.S.
β-blocker	3 (43%)	8 (73%)	2 (33%)	N.S.
Ca-blocker	1 (14%)	1 (9%)	0 (0%)	N.S.
Diuretics	4 (57%)	9 (82%)	4 (67%)	N.S.
Lipid-lowering drugs	2 (29%)	4 (36%)	2 (33%)	N.S.
Anti-diabetic drugs	2 (29%)	2 (18%)	0 (0%)	N.S.
Anti-arrhythmic drugs	4 (57%)	8 (73%)	4 (67%)	N.S.
Antidepressants	3 (43%)	3 (27%)	4 (67%)	N.S.
Swine	**Lean**	**MetS**		***p***
N	7	7		-
Weight (kg)	77 ± 4	110 ± 3		< 0.05
Age (years)	2.6 ± 0.1	2.8 ± 0.2		N.S.
Male/female	4/3	1/6		N.S.
SBP (mmHg)	82 ± 3	90 ± 5		< 0.05
DBP (mmHg)	59 ± 3	60 ± 5		N.S.
Fasting bG (mg/dL)	69 ± 3	80 ± 3		< 0.05
Total cholesterol (mg/dL)	80 ± 6	391 ± 108		< 0.05

Table 1 (continued)

	Non-ischemic		Ischemic	
Humans	**< 50% PB**	**50–75% PB**	**> 75% PB**	***p***
Triglycerides (mg/dL)	52 ± 6	67 ± 4		< 0.05

Data are presented as number (%) or mean ± SEM. *PB*, plaque burden; *SBP*, systolic blood pressure; *DBP*, diastolic blood pressure (humans conscious; swine under anesthesia); *LVAD*, left ventricular assistance device; *bG*, blood glucose; *HbA1c*, glycated hemoglobin; *HDL*, high-density lipoprotein; *ACEI*, angiotensin converting enzyme inhibitors; *ARB*, angiotensin II receptor blockers; *Ca*, calcium. MetS was defined by a blood pressure above 130/85 mmHg, a fasting blood glucose above 110 mg/dL, an HDL-C level below 40 mg/dL for men or below 50 mg/dL for women, a triglyceride level above 150 mg/dL, and a BMI above 30.0 kg/m^2. *N.S.*, not significant

coronary disease state. The argument could be made that this stratification reduces the differences between groups. However, while the clinical diagnosis of ischemic cardiomyopathy is an important predictor of 5-year mortality, the extent of CAD is a much better predictor of survival in heart failure patients [38]. Histology can be considered a "snapshot" of one specific cross section of the artery, not precisely indicative of total artery health. However, as both humans and Ossabaw swine with metabolic syndrome develop diffuse coronary plaque throughout the proximal, middle, and distal sections of the artery [21], the histology might be considered a *representative* snapshot of overall coronary health and plaque development. Therefore, basing human cohorts on coronary plaque burden seems to be a reasonable stratification strategy and the relative benefits and weaknesses of using clinical diagnosis versus coronary plaque burden should be

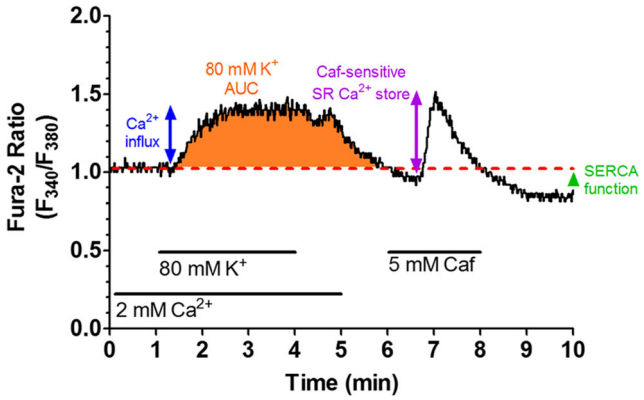

Fig. 2 Sample Ca^{2+} tracing showing the change in the F_{340}/F_{380} excitation fluorescence emission ratio from a human CSM cell. Treatments and duration are indicated by solid lines. Baseline Ca^{2+} values were established during the first minute in a physiological salt solution (red dashed line). Cell depolarization with an 80 mM K^+ solution initiated Ca^{2+} influx via voltage-gated Ca^{2+} channels. The height of the Ca^{2+} influx peak (blue arrow) and the area under the curve (AUC, orange area) were calculated to quantify Ca^{2+} influx activity. SR Ca^{2+} store was released by activating ryanodine receptors with 5 mM caffeine (Caf) and was measured by the height of the caffeine-induced peak (purple arrow). The undershoot from baseline was used to measure SERCA activity (green caret)

Table 2 Linear regression analyses for CSM $[Ca^{2+}]_i$ handling measures versus histology measurements and patient parameters

	Humans		Swine	
	p	***R***	***p***	***R***
Structural (histology) parameters				
Percent media vs.				
Ca^{2+} influx	0.01	0.51	0.48	0.22
80K AUC	0.03	0.44	0.45	0.24
SR store release	0.08	0.38	0.41	0.26
Intima/media ratio vs.				
Ca^{2+} influx	0.02	− 0.50	0.04	− 0.59
80K AUC	0.03	− 0.43	0.05	− 0.58
Percent total collagen vs.				
Ca^{2+} influx	0.01	− 0.51	0.04	− 0.60
80K AUC	< 0.01	− 0.60	0.12	− 0.47
SR store release	0.02	− 0.49	0.33	− 0.31
Percent calcification vs.				
Ca^{2+} influx	0.02	− 0.48	0.96	− 0.01
Patient clinical parameters				
BMI vs.				
Ca^{2+} influx	0.03	− 0.42	-	-
80K AUC	0.01	− 0.52	-	-
Age vs.				
SR store release	0.02	0.47	0.76	0.10
Number of MetS risk factors vs.				
80K AUC	0.01	− 0.51	-	-
LDL cholesterol vs.				
Ca^{2+} influx	0.01	− 0.48	-	-
Total cholesterol vs.				
Ca^{2+} influx	0.04	− 0.41	0.09	− 0.51

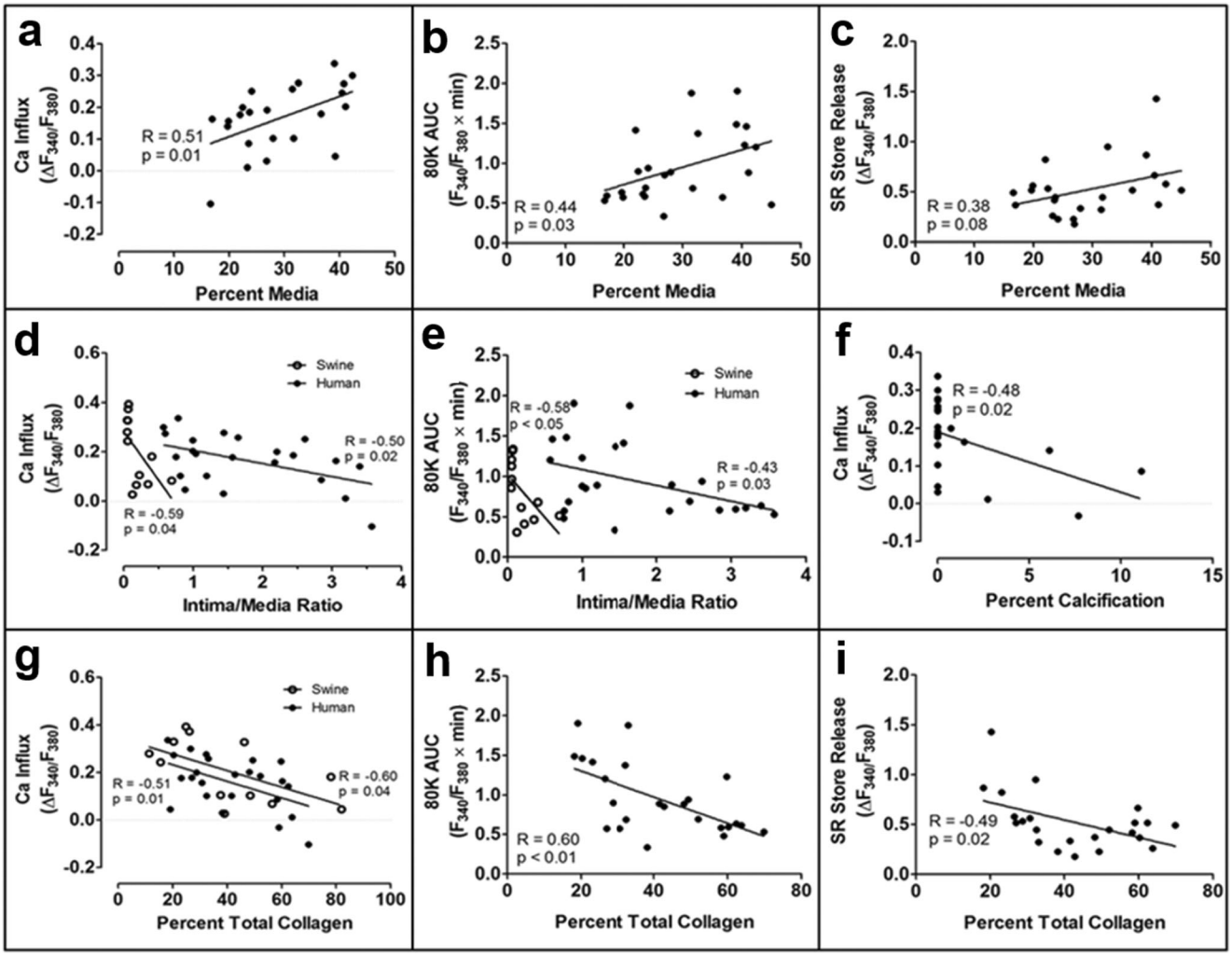

Fig. 3 Significant correlation of human coronary smooth muscle Ca^{2+} signaling to histological measures. The percent media (a–c), intima/media ratio (d–e), percent calcification (f), and percent collagen (g–i) were significantly correlated to Ca^{2+} influx (a, d, f, g), area under the 80 mM K^+ curve (b, e, h), and SR store release (c and i). Data points for swine (open circles) are included when the correlation was significant, as well (d, e, and g)

explored further to identify the more sound stratification strategy.

Patients in this study had different cardiac and CAD severities and similar clinical characteristics. It is important to note, however, that the patients have similarly increased cardiometabolic risk above healthy subjects. There is enough variability within all the groups that enabled excellent regression analysis. This allowed us to test for associations between cardiometabolic risk factors and $[Ca^{2+}]_i$ regulation. Additionally, we show that the number of MetS risk factors, as opposed to the diagnosis of MetS itself, affects $[Ca^{2+}]_i$ regulation. This is consistent with several studies on MetS and CAD [39–41]. One study found that Japanese patients with either dilated non-ischemic cardiomyopathy or ischemic cardiomyopathy have an incidence of MetS twice as frequently as the general population and have comparable metabolic components, indicating that the risk factors associated with MetS influence the etiology of both ischemic and non-ischemic cardiomyopathy [42].

It is important to note that over half of the patients in this study had left ventricular assist device (LVAD) support. LVADs deliver blood continuously from the left ventricle to the aorta, mechanically unloading the left ventricle and restoring total systemic blood pressure [43]. The continuous blood flow produced by LVAD support (as opposed to pulsatile flow accomplished with a native heartbeat) has several implications for regional flow

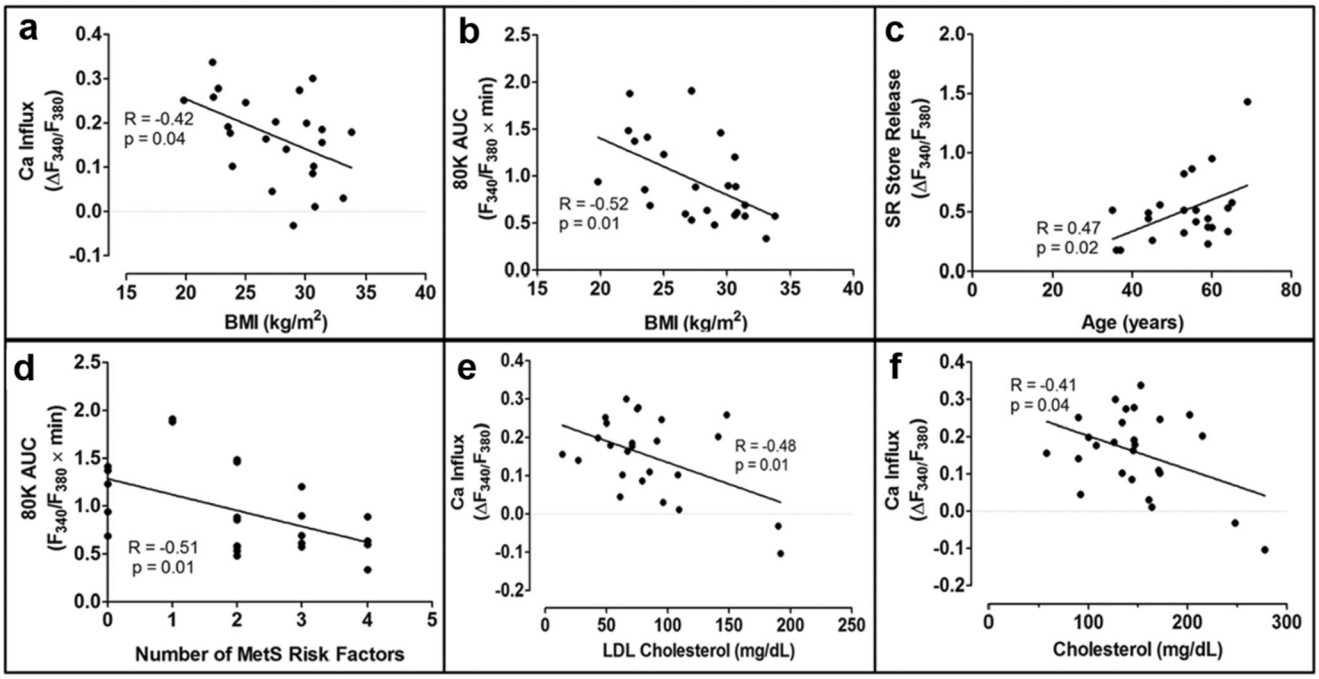

Fig. 4 Significant correlation of human coronary smooth muscle Ca^{2+} signaling to cardiometabolic patient data. Patient BMI (a and b), age (c), the number of MetS risk factors (d), and dyslipidemia (e–f) were correlated to Ca^{2+} influx (a, d, and e), area under the 80 mM K^+ curve (b and d), and SR store release (c)

dynamics, including coronary flow. In fact, implantation of a continuous flow LVAD is associated with a decrease in total coronary blood flow in a swine model [44]. While it appears that coronary artery endothelial function is not impaired by long-term LVAD support [45], the coronary arteries of human patients develop remodeling with increased fibrosis [46]. Intracellular Ca^{2+} changes in coronary smooth muscle usually accompany structural changes [16]. While studies have shown that LVAD support can increase Ca^{2+} cycling in cardiomyocytes [47], there have been no studies investigating coronary smooth muscle $[Ca^{2+}]_i$ handling in LVAD patients. Our study was not statistically powered to resolve a difference between patients with or without LVAD support. Therefore, it is difficult to determine exactly how LVAD support would affect $[Ca^{2+}]_i$ in coronary smooth muscle cells. This would be a promising research direction for future investigations.

Although humans and swine cannot and should not be directly compared, it is apparent that, while humans in general have a greater plaque burden than swine (Fig. 1m), swine exhibit more highly altered $[Ca^{2+}]_i$ handling in all the measured parameters (Fig. 5b–d). This may be due to the duration of the disease and severity of the risk factors. Atherosclerosis is a chronic disease occurring over several decades in the human population. Conversely, the Ossabaw swine with MetS-induced CAD are on a diet specifically designed to expedite plaque development over a time span of only 11 months, which would only be 7–10 years of a human lifespan. This could lead to more rapid changes in the cellular milieu, potentially causing more extreme adaptations in CSM leading to more severe $[Ca^{2+}]_i$ dysregulation, as compared to the slower, more chronic condition in humans. This also supports the concept that $[Ca^{2+}]_i$ dysregulation occurs before and perhaps triggers the structural changes in the artery.

There are limitations of this study. First, hearts from healthy humans without heart failure were not included due to scarcity of tissue. Therefore, this study indirectly compares arteries from pathological human hearts to physiologically healthy, lean swine. Our coronary plaque-based stratification of the severity of disease in the humans is not ideal. However, as we are concerned with relationships in $[Ca^{2+}]_i$ handling as a function of cardiometabolic risk and are not comparing these two species directly, we can still extrapolate from the data that the directional changes in $[Ca^{2+}]_i$ dysregulation patterns from a state of mild or no disease to a state of greater disease are maintained in both species. Finally, the major

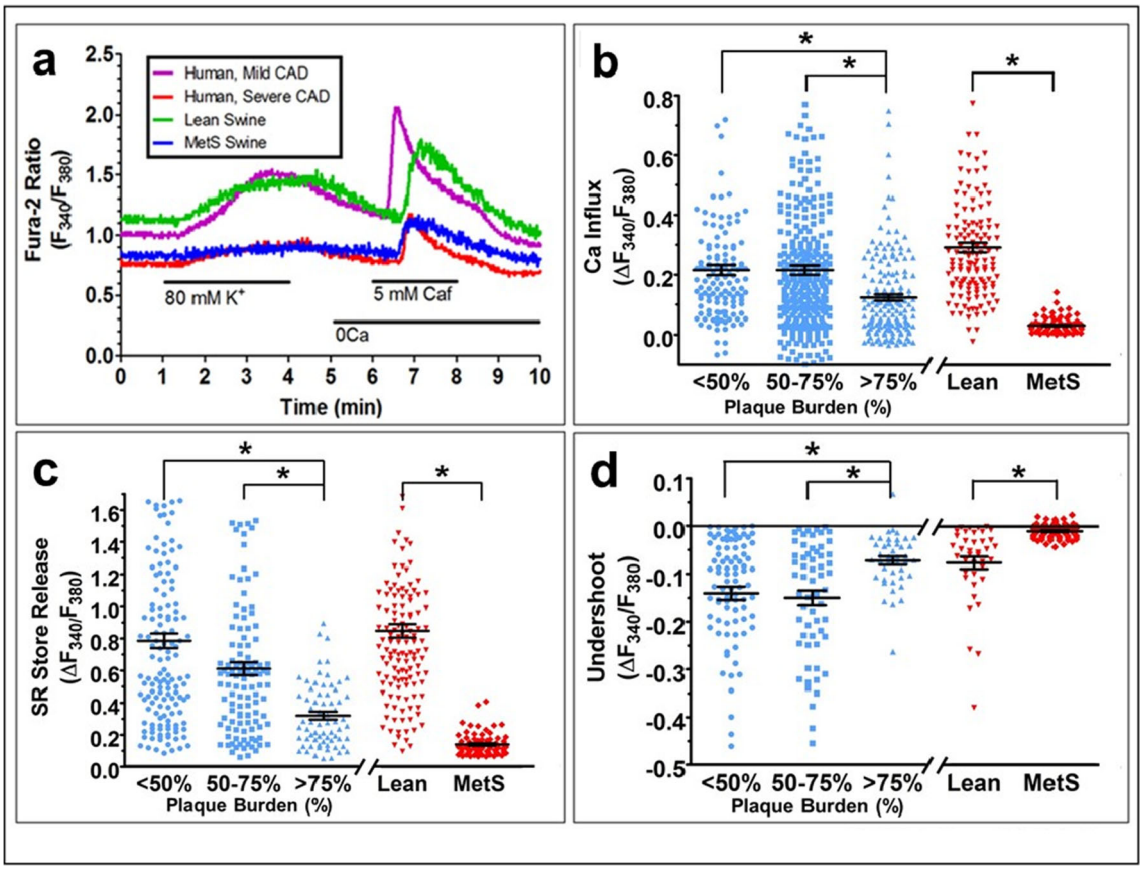

Fig. 5 Intracellular Ca^{2+} measures in CSM cells. Typical Ca^{2+} tracings show the change in the F_{340}/F_{380} excitation fluorescence emission ratio from human and swine CSM cells. There are similarities between humans with mild, non-ischemic CAD and lean swine and between humans with severe, ischemic CAD and MetS swine (a). Mild, non-ischemic CAD was defined by a plaque burden below 50%, while severe, ischemic CAD was defined by a plaque burden of over 75%. Both humans and swine with CAD exhibit decreased Ca^{2+} influx (b), SR Ca^{2+} store capacity (c), and SERCA function (d). Group data are plotted as mean ± SE with black lines and bars; individual cells are show in blue symbols for humans and red symbols for swine

weakness of this study is the relatively small human sample set, which affects the generalizability of these results. Future studies should expand on these findings by including a greater number of patients.

An adequate animal model for macrovascular coronary artery disease and subsequent heart failure is of utmost importance, as a better understanding of the pathophysiology of cardiomyopathies could lead to the development of more effective heart failure therapeutics. This report is the first characterization of $[Ca^{2+}]_i$ dysregulation in freshly harvested CSM from explanted human hearts. The data strongly support the clinical relevance of the Ossabaw miniature swine model of MetS and CAD. A reliable, clinically relevant animal model that recapitulates human disease on a cellular level provides far more confidence of the translatability of the data.

Abbreviations BMI, Body mass index; $[Ca^{2+}]_i$, Intracellular free calcium; CSM, Coronary smooth muscle; CAD, Coronary artery disease; LDL, Low-density lipoprotein; LVAD, Left ventricular assist device; MetS, Metabolic syndrome; SERCA, Sarco-endoplasmic reticulum Ca^{2+} ATPase; SR, Sarcoplasmic reticulum

Acknowledgements The authors acknowledge the Indiana University School of Medicine Histology Core and Dr. Keith Condon for processing the histology and use of their equipment. Jill K. Badin's Ph.D. thesis dated August 2019 contained some of the data in this manuscript and can be found at: https://scholarworks.iupui.edu/bitstream/handle/1805/20549/Badin_iupui_0104D_10379.pdf?isAllowed=y&sequence=1

Author Contribution J.K.B., S.D.R., and M.S. are responsible for conception and design of research; J.K.B., C.E., S.D.R., M.A., Z.A.H., I.W., and J.P.G. performed experiments; J.K.B., C.E., and S.D.R. analyzed data; J.K.B., C.E., and M.S. interpreted results of experiments; J.K.B., C.E., and M.S. prepared figures; J.K.B. and C.E. drafted manuscript; J.K.B., C.E., and M.S. edited and revised manuscript; J.K.B., C.E.,

S.D.R., M.A., Z.A.H., I.W., J.P.G., and M.S. approved the final version of the manuscript.

Funding This research was funded by the National Institutes of Health HL125385, P30 DK097512, the Joshua Diabetes Research Fund, and the Indiana University School of Medicine Center of Excellence in Cardiovascular Research.

Declarations

Ethics Approval for Use of Animals All institutional and national guidelines for the care and use of laboratory animals were followed and approved by the Institutional Animal Care and Use Committee at the Indiana University School of Medicine.

Ethics Approval for Human Subjects This article does not contain any studies with human participants performed by any of the authors, as approved by exemption, per the use of discarded human tissue, by the Indiana University Institutional Review Board.

Conflict of Interest The authors declare no competing interests.

References

1. Benjamin, E. J., Virani, S. S., Callaway, C. W., Chamberlain, A. M., Chang, A. R., Cheng, S., et al. (2018). Heart Disease and stroke statistics-2018 update: A report from the American Heart Association. *Circulation, 137*(12), e67–e492. https://doi.org/10.1161/CIR.0000000000000558.
2. Wexler, R. K., Elton, T., Pleister, A., & Feldman, D. (2009). Cardiomyopathy: An overview. *American Family Physician, 79*(9), 778–784.
3. Libby, P., Ridker, P. M., & Hansson, G. K. (2011). Progress and challenges in translating the biology of atherosclerosis. *Nature, 473*(7347), 317–325. https://doi.org/10.1038/nature10146.
4. Owens, G. K., Kumar, M. S., & Wamhoff, B. R. (2004). Molecular regulation of vascular smooth muscle cell differentiation in development and disease. *Physiological Reviews, 84*(3), 767–801. https://doi.org/10.1152/physrev.00041.2003.
5. van der Schaaf, R. J., Timmer, J. R., Ottervanger, J. P., Hoorntje, J. C., de Boer, M. J., Suryapranata, H., et al. (2006). Long-term impact of multivessel disease on cause-specific mortality after ST elevation myocardial infarction treated with reperfusion therapy. *Heart, 92*(12), 1760–1763. https://doi.org/10.1136/hrt.2005.086058.
6. Mozaffarian, D., Benjamin, E. J., Go, A. S., Arnett, D. K., Blaha, M. J., Cushman, M., et al. (2016). Heart Disease and stroke statistics-2016 update: A report from the American Heart Association. *Circulation, 133*(4), e38–e60. https://doi.org/10.1161/CIR.0000000000000350.
7. Karwowski, W., Naumnik, B., Szczepanski, M., & Mysliwiec, M. (2012). The mechanism of vascular calcification - A systematic review. *Medical Science Monitor, 18*(1), RA1–RA11.
8. Hill-Eubanks, D. C., Werner, M. E., Heppner, T. J., & Nelson, M. T. (2011). Calcium signaling in smooth muscle. *Cold Spring Harbor Perspectives in Biology, 3*(9), a004549. https://doi.org/10.1101/cshperspect.a004549.
9. Wamhoff, B. R., Bowles, D. K., McDonald, O. G., Sinha, S., Somlyo, A. P., Somlyo, A. V., et al. (2004). L-type voltage-gated Ca2+ channels modulate expression of smooth muscle differentiation marker genes via a rho kinase/myocardin/SRF-dependent mechanism. *Circulation Research, 95*(4), 406–414. https://doi.org/10.1161/01.RES.0000138582.36921.9e.
10. Lundberg, M. S., Curto, K. A., Bilato, C., Monticone, R. E., & Crow, M. T. (1998). Regulation of vascular smooth muscle migration by mitogen-activated protein kinase and calcium/calmodulin-dependent protein kinase II signaling pathways. *Journal of Molecular and Cellular Cardiology, 30*(11), 2377–2389. https://doi.org/10.1006/jmcc.1998.0795.
11. Pauly, R. R., Bilato, C., Sollott, S. J., Monticone, R., Kelly, P. T., Lakatta, E. G., et al. (1995). Role of calcium/calmodulin-dependent protein kinase II in the regulation of vascular smooth muscle cell migration. *Circulation, 91*(4), 1107–1115. https://doi.org/10.1161/01.cir.91.4.1107.
12. House, S. J., Potier, M., Bisaillon, J., Singer, H. A., & Trebak, M. (2008). The non-excitable smooth muscle: Calcium signaling and phenotypic switching during vascular disease. *Pflügers Archiv, 456*(5), 769–785. https://doi.org/10.1007/s00424-008-0491-8.
13. Kruse, H. J., Bauriedel, G., Heimerl, J., Hofling, B., & Weber, P. C. (1994). Role of L-type calcium channels on stimulated calcium influx and on proliferative activity of human coronary smooth muscle cells. *Journal of Cardiovascular Pharmacology, 24*(2), 328–335.
14. Nilsson, J., Sjolund, M., Palmberg, L., Von Euler, A. M., Jonzon, B., & Thyberg, J. (1985). The calcium antagonist nifedipine inhibits arterial smooth muscle cell proliferation. *Atherosclerosis, 58*(1-3), 109–122. https://doi.org/10.1016/0021-9150(85)90059-0.
15. Jiang, H., & Stephens, N. L. (1994). Calcium and smooth muscle contraction. *Molecular and Cellular Biochemistry, 135*(1), 1–9. https://doi.org/10.1007/BF00925956.
16. Sturek, M. (2011). Ca^{2+} regulatory mechanisms of exercise protection against coronary artery disease in metabolic syndrome and diabetes. *Journal of Applied Physiology, 111*(2), 573–586. https://doi.org/10.1152/japplphysiol.00373.2011.
17. Witczak, C. A., Wamhoff, B. R., & Sturek, M. (2006). Exercise training prevents Ca^{2+} dysregulation in coronary smooth muscle from diabetic dyslipidemic Yucatan swine. *Journal of Applied Physiology, 101*(3), 752–762. https://doi.org/10.1152/japplphysiol.00235.2006.
18. Berwick, Z. C., Dick, G. M., O'Leary, H. A., Bender, S. B., Goodwill, A. G., Moberly, S. P., et al. (2013). Contribution of electromechanical coupling between Kv and Ca v1.2 channels to coronary dysfunction in obesity. *Basic Research in Cardiology, 108*(5), 370. https://doi.org/10.1007/s00395-013-0370-0.
19. Edwards, J. M., Neeb, Z. P., Alloosh, M. A., Long, X., Bratz, I. N., Peller, C. R., et al. (2010). Exercise training decreases store-operated Ca^{2+} entry associated with metabolic syndrome and coronary atherosclerosis. *Cardiovascular Research, 85*(3), 631–640. https://doi.org/10.1093/cvr/cvp308.
20. Hill, B. J., Price, E. M., Dixon, J. L., & Sturek, M. (2003). Increased calcium buffering in coronary smooth muscle cells from diabetic dyslipidemic pigs. *Atherosclerosis, 167*(1), 15–23. https://doi.org/10.1016/s0021-9150(02)00381-7.
21. Neeb, Z. P., Edwards, J. M., Alloosh, M., Long, X., Mokelke, E. A., & Sturek, M. (2010). Metabolic syndrome and coronary artery disease in Ossabaw compared with Yucatan swine. *Comparative Medicine, 60*(4), 300–315.
22. McKenney-Drake, M. L., Rodenbeck, S. D., Owen, M. K., Schultz, K. A., Alloosh, M., Tune, J. D., et al. (2016). Biphasic alterations in coronary smooth muscle Ca2+ regulation in a repeat cross-sectional study of coronary artery disease severity in metabolic syndrome. *Atherosclerosis, 249*, 1–9. https://doi.org/10.1016/j.atherosclerosis.2016.03.032.
23. Sturek, M., Alloosh, M., & Sellke, F. W. (2020). Swine disease models for optimal vascular engineering. *Annual Review of Biomedical Engineering, 22*, 25–49. https://doi.org/10.1146/annurev-bioeng-082919-053009.

24. Badin, J. K., Bruning, R. S., & Sturek, M. (2018). Effect of metabolic syndrome and aging on Ca^{2+} dysfunction in coronary smooth muscle and coronary artery disease severity in Ossabaw miniature swine. *Experimental Gerontology, 108*, 247–255. https://doi.org/10.1016/j.exger.2018.04.024.
25. Badin, J. K., Kole, A., Stivers, B., Progar, V., Pareddy, A., Alloosh, M., et al. (2018). Alloxan-induced diabetes exacerbates coronary atherosclerosis and calcification in Ossabaw miniature swine with metabolic syndrome. *Journal of Translational Medicine, 16*(1), 58. https://doi.org/10.1186/s12967-018-1431-9.
26. Institute for Laboratory Animal Research. (2010). *Guide for the care and use of laboratory animals*. National Academy Press.
27. AVMA Panel on Euthanasia.American Veterinary Medical Association. (2001). 2000 report of the AVMA panel on euthanasia. *JAVMA, 218*, 669–696.
28. Grynkiewicz, G., Poenie, M., & Tsien, R. Y. (1985). A new generation of Ca^{2+} indicators with greatly improved fluorescence properties. *J.Biol.Chem., 260*, 3440–3450.
29. Oliver, A. E., Baker, G. A., Fugate, R. D., Tablin, F., & Crowe, J. H. (2000). Effects of temperature on calcium-sensitive fluorescent probes. *Biophysical Journal, 78*(4), 2116–2126. https://doi.org/10.1016/S0006-3495(00)76758-0.
30. Dineen, S. L., McKenney, M. L., Bell, L. N., Fullenkamp, A. M., Schultz, K. A., Alloosh, M., et al. (2015). Metabolic syndrome abolishes glucagon-like peptide 1 receptor agonist stimulation of SERCA in coronary smooth muscle. *Diabetes, 64*(9), 3321–3327. https://doi.org/10.2337/db14-1790.
31. McKenney-Drake, M. L., Territo, P. R., Salavati, A., Houshmand, S., Persohn, S., Liang, Y., et al. (2016). ^{18}F-NaF PET imaging of early coronary artery calcification. *JACC: Cardiovascular Imaging, 9*, 627–628. https://doi.org/10.1016/j.jcmg.2015.02.026.
32. Rodenbeck, S. D., Zarse, C. A., McKenney-Drake, M. L., Bruning, R. S., Sturek, M., Chen, N. X., et al. (2017). Intracellular calcium increases in vascular smooth muscle cells with progression of chronic kidney disease in a rat model. *Nephrology, Dialysis, Transplantation, 32*(3), 450–458. https://doi.org/10.1093/ndt/gfw274.
33. Bobe, R., Hadri, L., Lopez, J. J., Sassi, Y., Atassi, F., Karakikes, I., et al. (2011). SERCA2a controls the mode of agonist-induced intracellular Ca2+ signal, transcription factor NFAT and proliferation in human vascular smooth muscle cells. *Journal of Molecular and Cellular Cardiology, 50*(4), 621–633. https://doi.org/10.1016/j.yjmcc.2010.12.016.
34. Karagiannis, G. S., Weile, J., Bader, G. D., & Minta, J. (2013). Integrative pathway dissection of molecular mechanisms of moxLDL-induced vascular smooth muscle phenotype transformation. *BMC Cardiovascular Disorders, 13*, 4. https://doi.org/10.1186/1471-2261-13-4.
35. Spillmann, F., Miteva, K., Pieske, B., Tschope, C., & Van Linthout, S. (2015). High-density lipoproteins reduce endothelial-to-mesenchymal transition. *Arteriosclerosis, Thrombosis, and Vascular Biology, 35*(8), 1774–1777. https://doi.org/10.1161/ATVBAHA.115.305887.
36. Wang, Y., Ji, L., Jiang, R., Zheng, L., & Liu, D. (2014). Oxidized high-density lipoprotein induces the proliferation and migration of vascular smooth muscle cells by promoting the production of ROS. *Journal of Atherosclerosis and Thrombosis, 21*(3), 204–216. https://doi.org/10.5551/jat.19448.
37. Gheorghiade, M., & Bonow, R. O. (1998). Chronic heart failure in the United States: a manifestation of coronary artery disease. *Circulation, 97*(3), 282–289. https://doi.org/10.1161/01.cir.97.3.282.
38. Bart, B. A., Shaw, L. K., McCants Jr., C. B., Fortin, D. F., Lee, K. L., Califf, R. M., et al. (1997). Clinical determinants of mortality in patients with angiographically diagnosed ischemic or nonischemic cardiomyopathy. *Journal of the American College of Cardiology, 30*(4), 1002–1008. https://doi.org/10.1016/s0735-1097(97)00235-0.
39. Kim, J. Y., Mun, H. S., Lee, B. K., Yoon, S. B., Choi, E. Y., Min, P. K., et al. (2010). Impact of metabolic syndrome and its individual components on the presence and severity of angiographic coronary artery disease. *Yonsei Medical Journal, 51*(5), 676–682. https://doi.org/10.3349/ymj.2010.51.5.676.
40. Gui, M. H., Ling, Y., Liu, L., Jiang, J. J., Li, X. Y., & Gao, X. (2017). Effect of metabolic syndrome score, metabolic syndrome, and its individual components on the prevalence and severity of angiographic coronary artery disease. *Chinese Medical Journal (England), 130*(6), 669–677. https://doi.org/10.4103/0366-6999.201611.
41. Ahmadi, A., Leipsic, J., Feuchtner, G., Gransar, H., Kalra, D., Heo, R., et al. (2015). Is metabolic syndrome predictive of prevalence, extent, and risk of coronary artery disease beyond its components? Results from the multinational coronary CT angiography evaluation for clinical outcome: An international multicenter registry (CONFIRM). *PLoS One, 10*(3), e0118998. https://doi.org/10.1371/journal.pone.0118998.
42. Miura, Y., Fukumoto, Y., Shiba, N., Miura, T., Shimada, K., Iwama, Y., et al. (2010). Prevalence and clinical implication of metabolic syndrome in chronic heart failure. *Circulation Journal, 74*(12), 2612–2621. https://doi.org/10.1253/circj.cj-10-0677.
43. Klotz, S., Jan Danser, A. H., & Burkhoff, D. (2008). Impact of left ventricular assist device (LVAD) support on the cardiac reverse remodeling process. *Progress in Biophysics and Molecular Biology, 97*(2-3), 479–496. https://doi.org/10.1016/j.pbiomolbio.2008.02.002.
44. Ootaki, Y., Kamohara, K., Akiyama, M., Zahr, F., Kopcak Jr., M. W., Dessoffy, R., et al. (2005). Phasic coronary blood flow pattern during a continuous flow left ventricular assist support. *European Journal of Cardio-Thoracic Surgery, 28*(5), 711–716. https://doi.org/10.1016/j.ejcts.2005.08.008.
45. Symons, J. D., Deeter, L., Deeter, N., Bonn, T., Cho, J. M., Ferrin, P., et al. (2019). Effect of continuous-flow left ventricular assist device support on coronary artery endothelial function in ischemic and nonischemic cardiomyopathy. *Circulation: Heart Failure, 12*(8), e006085. https://doi.org/10.1161/CIRCHEARTFAILURE.119.006085.
46. Ambardekar, A. V., Weiser-Evans, M. C. M., Li, M., Purohit, S. N., Aftab, M., Reece, T. B., et al. (2018). Coronary artery remodeling and fibrosis with continuous-flow left ventricular assist device support. *Circulation: Heart Failure, 11*(5), e004491. https://doi.org/10.1161/CIRCHEARTFAILURE.117.004491.
47. Wei, X., Li, T., Hagen, B., Zhang, P., Sanchez, P. G., Williams, K., et al. (2013). Short-term mechanical unloading with left ventricular assist devices after acute myocardial infarction conserves calcium cycling and improves heart function. *JACC: Cardiovascular Interventions, 6*(4), 406–415. https://doi.org/10.1016/j.jcin.2012.12.122.